NASA TECHNICAL MEMORANDUM

NASA TM X-1371

NASA TM X-1371

EXPERIMENTAL INVESTIGATION OF BASE FLOW FIELD AT HIGH ALTITUDES FOR CONFIGURATIONS OF FOUR AND FIVE CLUSTERED NOZZLES

by R. A. Wasko and T. L. Cover

Lewis Research Center

Cleveland, Ohio

NATIONAL AERONAUTICS AND SPACE ADMINISTRATION • WASHINGTON, D. C. • MAY 1967

NASA TM X-1371

EXPERIMENTAL INVESTIGATION OF BASE FLOW FIELD AT HIGH ALTITUDES FOR CONFIGURATIONS OF FOUR AND FIVE CLUSTERED NOZZLES

By R. A. Wasko and T. L. Cover

Lewis Research Center
Cleveland, Ohio

NATIONAL AERONAUTICS AND SPACE ADMINISTRATION

For sale by the Clearinghouse for Federal Scientific and Technical Information
Springfield, Virginia 22151 - CFSTI price $3.00

EXPERIMENTAL INVESTIGATION OF BASE FLOW FIELD AT HIGH ALTITUDES FOR CONFIGURATIONS OF FOUR AND FIVE CLUSTERED NOZZLES

by R. A. Wasko and T. L. Cover

Lewis Research Center

SUMMARY

An experimental investigation of the base flow field for four- and five-nozzle-cluster configurations was made at altitudes from 60 000 to 200 000 feet, utilizing conical and contoured cold flow nozzles. Measurements of flow-field Mach number with translating probes indicated that in the center of the extended four-nozzle clusters, the reverse flow Mach number increased in magnitude with increasing nozzle-pressure ratio (i.e., nozzle-exit to ambient-static-pressure ratio) for both conical and contoured nozzles. Values ranged from completely subsonic flow for low pressure ratios to almost completely supersonic flow for high pressure ratios. When supersonic flow existed, the reverse flow then decelerated to subsonic velocities and stagnated at the base. Apparently this deceleration occurred through dissipation of the flow by mixing and shear forces since evidence of a normal shock was not observed. Flow angularity measurements in the vent area indicated that the curvature of the flow field decreased as nozzle-pressure ratio increased because of the increased strength of the reverse flow. Mach number variation in the center area with unextended nozzles was similar to that downstream of the nozzle-exit plane for the extended-nozzle configuration, but supersonic reverse flow decelerated through a normal shock because of the proximity of the base. The magnitude of the flow-field Mach number for the five-nozzle cluster was less than that of the four-nozzle cluster.

The flow-field total pressure for the four-nozzle-cluster configuration decreased towards the base in contrast to previous assumptions of a constant total pressure in the reverse flow. The magnitude of this loss in total pressure increased with increases in nozzle-pressure ratio. Base pressures for contoured-nozzle configurations were less than those of conical nozzle configurations at a given altitude and nozzle-pressure ratio and the nozzle-pressure ratio at which the base flow choked was higher. Similarly, nozzle gimbal decreased the base pressure and increased the choking nozzle-pressure ratio. Reductions in the nozzle extension from the base plate resulted in increased base pressure and reduced the choking nozzle-pressure ratio. The five-nozzle configuration had lower base pressures than the four-nozzle configurations at a given altitude and nozzle-pressure ratio, and choking occurred at a higher nozzle-pressure ratio.

INTRODUCTION

The base-flow phenomena of multinozzle configurations are of such complexity that present analytical techniques are limited in obtaining quantitative estimates of base pressure and convective heating rates. Hence, experimental studies are still necessary. The works of Korst and Goethert (refs. 1 to 3) remain in the major analytical contributions in this area. More recently, experimental studies (ref. 4) have indicated that the base flow may be even more complex than presumed in these analyses in that the reversed flow may be supersonic at high pressure ratios. The present experimental study is intended to examine more closely the details of the base flow at these high pressure ratios.

Cold flow models of four- and five-nozzle-cluster configurations were tested in the Lewis 10- by 10-foot supersonic wind tunnel at altitudes from 60 000 to 200 000 feet and nozzle-exit- to ambient-static-pressure ratios (hereinafter called nozzle-pressure ratio) from 2.5 to 4300. The model mounted in the test section is shown in figure 1. Free-stream effects were minimized by installing the nozzles in the base of a cone-cylinder-flare forebody. Geometric variables included conical and contoured nozzles, nozzle gimbal, and nozzle extension beyond the base.

Translating conical and pitot-static probes provided local Mach number, flow angles, and total pressures at discrete positions from the base plate to a point near the jet intersections. The flow field for the four-nozzle clusters was surveyed in the center and the lateral areas between the nozzles, whereas the five-nozzle cluster was surveyed in the lateral area only. In addition, base-plate static pressures were obtained for all configurations.

SYMBOLS

D_E nozzle-exit diameter, in.

M_E nozzle-exit Mach number

M_L local Mach number

M_O free-stream Mach number

P_C nozzle chamber pressure, psia

p_A ambient pressure measured on outer region of forebody base, psia

p_B base pressure, psia

p_E nozzle-exit static pressure, psia

$p_{t,1}$ probe total pressure (pitot pressure corrected for normal shock loss), psia

$p_{t,2}$ probe pitot pressure, psia

p_w wake pressure, psia

p_α static pressure measured on leeward side of probe conical surface

p_β static pressure measured on windward side of probe conical surface

S nozzle extension beyond base, in.

X distance of probe tip from base plate, in.

α flow angle, deg

γ ratio of specific heats

θ_E nozzle-exit angle, deg

APPARATUS

Configurations

Details of the four-nozzle base configurations are shown in figure 2. Contoured and conical nozzles were used, and both had an area ratio of 25. The nozzles were equally spaced about the circumference of a 2.5-inch circle and were mounted in a 5-inch-diameter plate that fit flush within the base of the cone-cylinder-flare forebody. The extended-nozzle configuration, shown in figure 2(a), had the nozzle-exit plane located 1.5 inches from the base plate (i.e., $S/D_E = 1.2$). The gimbaled-nozzle configuration shown in figure 2(b) provided a 6^o outward gimbal for the contoured nozzles. The unextended-nozzle configuration (i.e., $S/D_E = 0$) is shown in figure 2(c). An additional plate was attached to the forebody base and mounted flush with the exit plane of both the contoured- and conical-nozzle configurations.

Details of the five-nozzle configuration are shown in figure 3. Conical nozzles were used that had an area ratio of 4.92. Four nozzles equally spaced about the circumference of a 3.25-inch-diameter circle plus one nozzle in the center were mounted on a 7.0-inch-diameter plate. For this configuration, the nozzle-extension ratio S/D_E was 2.0. This base geometry nominally simulates the nozzle spacing and extension ratio of the Saturn S-IC booster.

Nozzle internal design details are shown in figure 4. For the four-nozzle clusters, contoured-nozzle details and coordinates are shown in figure 4(a), and conical nozzles are shown in figure 4(b). Although the conical nozzles were 2.25 inches long, they were so mounted in the base that the nozzle exit extended 1.5 inches beyond the base plate and

thus maintained the same S/D_E of 1.2 as the contoured nozzles.

Conical nozzles used in the five-nozzle cluster test are shown in figure 4(c). These nozzles were designed using the Goethert similarity parameter to simulate the F-1 engines used on the S-IC booster. This parameter discussed in reference 3 enables the use of a high-pressure air model to obtain similar base pressures as with hot jet models and states that the following conditions must be observed:

$$\left.\frac{\gamma M_E^2}{\sqrt{M_E^2 - 1}}\right|_{\text{COLD}} = \left.\frac{\gamma M_E^2}{\sqrt{M_E^2 - 1}}\right|_{\text{HOT}} \tag{1}$$

$$p_E \text{ cold} = p_E \text{ hot} \tag{2}$$

$$\theta_E \text{ cold} = \theta_E \text{ hot} \tag{3}$$

Equation (1) was used to obtain the model M_E and the resultant nozzle-area ratio 4.92. Equation (2) and the area ratio effectively describe the required cold-flow chamber pressure, which was computed to be 330 psi.

Instrumentation

Base-plate pressures were obtained with the instrumentation shown in figure 5. Static-pressure orifice distribution on the base of the cone-cylinder-flare forebody is shown in figure 5(a), while the distribution on the four-nozzle base plate is shown in figure 5(b). Also shown is a pressure orifice p_E located at the nozzle-exit plane, used to measure nozzle-exit pressure. Orifice distribution on the five-nozzle base plate is shown in figure 5(c).

Measurements of flow conditions were made with probes located as shown photographically in figure 6 and diagrammatically in figure 7. Probe locations for the four-nozzle cluster are shown in figure 6(a). One conical probe was located in the center of the four nozzles and measured Mach number and total pressure of the flow normal to the base. Another conical probe was located in the lateral area between the nozzles and measured flow conditions parallel to the base at the center of the minimum area between nozzles, hereinafter called the vent area. A pitot-static probe located in another lateral area measured conditions normal to the base in the vent area. The probes traversed equal distances, thus each probe measured flow quantities at the same discrete station

above the base (i.e., the same X/S).

Probe locations for the five-nozzle cluster are shown in figure 6(b). A conical probe was located in the lateral area at the minimum point between nozzles (vent area) and measured conditions parallel to the base, while a pitot-static probe identically located in a different quadrant measured conditions normal to the base.

Design details of these probes are shown in figure 7. Standard design procedure was used for the pitot-static probe. Four surface static orifices equally spaced around the circumference were manifolded to yield an average surface static pressure. For the conical probe, four surface static orifices were located on the conical surface such that a pair was placed in each of two orthogonal planes, coincident and normal to the plane containing the line of survey and the centerline of the cluster.

PROCEDURE

For this test, the Lewis 10- by 10-foot supersonic wind tunnel was, in effect, used as an ejector pump to provide a low-pressure environment for the nozzle flow. Tunnel Mach number was varied from 2.0 to 3.5 to provide a tunnel pressure altitude variation from 60 000 to 150 000 feet. This variation provided a jet on base-plate ambient pressure corresponding to altitudes from 60 000 to 200 000 feet. Interactions of the jet flow with the free stream were prevented by locating the nozzles in the dead-air region of the forebody base. Thus, the effect of these interactions on the nozzle-base flow field was eliminated for both high and low nozzle-pressure ratios.

High-pressure dried air was used to provide nozzle flow at chamber pressures of 1000, 1500, and 2000 psia for the four-nozzle cluster, and 500, 330, and 150 psia for the five-nozzle cluster. At a given setting of free-stream conditions and probe position, the nozzle flow was initiated to establish the desired value of chamber pressure, and the forebody base-plate static probes were monitored to ensure that steady-state base flow conditions were achieved prior to data recording. The outermost static pressure was found to be representative of the pressure environment in the forebody base and was chosen as the ambient pressure.

For analysis of the conical probe results, a calibration of Mach number and flow angularity was obtained for the probe in the Lewis 8- by 6-foot transonic wind tunnel at Mach numbers from 0.56 to 1.95 and angles of attack up to 33.5°. Results are presented in figure 8 wherein conical surface static pressure measured on the leeward side of the probe p_{α} is ratioed to the pitot pressure $p_{t,2}$ and is plotted as a function of a similar ratio for a surface static pressure located on the windward side p_{β}. The map was extrapolated to Mach numbers greater than 1.95 and 0° flow angle by using flow tables for cones at small angles of attack (ref. 5). Substantial agreement can be

seen between the theory and the calibration results. The map was extrapolated for Mach numbers less than 0.56 and flow angles up to 33.5° by the following procedure: The theoretical line for 0° flow angle was extended to a point where the surface- to total-pressure ratio was 1 (i.e., $M_0 = 0$). Lines of constant flow angle other than 0° were similarly extended to intersect this point. Lines of constant Mach number were determined by an intermediate procedure wherein the variation of static- to total-pressure ratio with Mach numbers greater than 0.56 was plotted from the calibration data for $\alpha = 0^{\circ}$. The resultant curve, not shown in this report, was so extrapolated to $M_0 = 0$ that values of static- to total-pressure ratio could be obtained for discrete Mach numbers less than 0.56. These values were located on the calibration curve for $\alpha = 0^{\circ}$, and proportionate distances from the $M_0 = 0$ point were located on curves for angles other than 0°.

In the center region of the four-nozzle cluster, flow angularity relative to the probe axis was negligible, and the Mach number was easily obtained from the calibration curve. Total pressure of the reverse flow was then calculated from the Mach number, measured pitot pressure, and normal shock relations. In the vent area, however, the flow angularity changes from a direction normal to the base at the jet intersection to a parallel direction at the base surface. Since the conical-probe axis was parallel to the base plate, the conical-probe measurements were found to be within the calibration range of 0° to 33.5° at positions close to the base but beyond it near the nozzle-exit plane. Consequently, the calibration was used for conical-probe positions near the base wherever possible. At positions where the angularity calibration was exceeded, Mach number was computed from measurements made with both the conical and the pitot-static probe in the following manner: The pitot pressure from the pitot-static probe, which was normal to the base, was assumed to be the local pitot pressure; and the pitot pressure from the conical probe was assumed to be the corresponding local static pressure. The Mach number at this position then was calculated from the ratio of the assumed pitot to static pressure using the Rayleigh equation. This procedure obviously becomes less accurate as the flow angularity varies from 90° to 33°, but nevertheless the procedure was adequate to determine the flow field qualitatively.

RESULTS AND DISCUSSION

A theoretical flow model for the interaction of clustered, underexpanded jets is shown in figure 9 and is obtained from a concept presented in reference 6. The exhaust gases expand through the nozzles from chamber conditions to nozzle-exit conditions p_E and M_E. The external jet expansion produces a divergent plume, and a mutual impingement occurs downstream of the nozzle-exit plane. As a result of this impinge-

ment the supersonic gases are deflected, producing a trailing shock and a wake pressure p_w associated with this shock. Within the mixing boundary of each jet is a separating streamline so defined that the integrated flow rate inside it is equal to the flow rate of the nozzle. That portion of the nozzle flow that has enough total pressure to negotiate the rise in static pressure in the wake, passes downstream. The portion that cannot pass downstream is turned and flows into the base. Therefore, a stagnation streamline must exist that distinguishes the flow passing downstream from that recirculated into the base. This stagnation streamline is called the limiting streamline. The recirculated mass flows into the center area in a flow passage formed by the jet plume boundaries and the nozzle external walls and flows out of the base through the vent area between the nozzles.

Results of a study wherein pressure measurements were made of the reverse flow in the center of a four-nozzle cluster by means of a traversing pitot probe are given in reference 4. The reverse flow local Mach number was calculated from these measurements by assuming that the total pressure of the reverse flow was constant. Thus, the flow accelerated continuously from Mach 1.0 in the region bounded by the jet plumes to supersonic velocities. A normal shock was assumed to exist near the base, resulting from the deceleration of this supersonic flow as it impinged at the center of the base. A varying total pressure, however, would obviate interpretation of pitot probe pressure measurements and calculation of reverse flow Mach number. The typical velocity profile of the flow model shows that at a given axial location within the region downstream of the jet exit, the total pressure of the reverse flow will vary radially in a manner similar to the velocity profile. A centerline measurement would then represent the maximum total pressure at that distance from the base. As the flow approaches the base, internal shear forces and turbulent mixing will act to dissipate the total pressure. Thus, measurements made on the centerline should decrease towards the base from a maximum value nearly equal to the wake static pressure. The flow velocities would depend on the magnitude of the reverse flow total pressure, static pressure, and flow passage geometry. These variables are of course dependent on exit Mach number and nozzle-pressure ratio which determine the wake pressure rise and plume shape. Therefore, subsonic and/or supersonic flow velocities may exist. Furthermore, the internal shear and mixing could decelerate the flow to subsonic speeds without a normal shock, provided sufficient length exists for this deceleration to occur. (This type of deceleration is shown to be theoretically and experimentally possible in reference 7 for an axially symmetrical compressible jet mixing with quiescent air.) If sufficient length is not available, a normal shock may stand off from the base plate to cause an abrupt deceleration to subsonic speeds.

The results of this study will define flow conditions; that is, Mach number, flow angle, and total pressure in the center of both the vent area and the center area. The

use of a calibrated conical probe, however, eliminated assumptions concerning the reverse flow total pressure and yielded Mach number directly. Since the probe calibration was obtained in a uniform flow field, some error may result when it is used in a nonuniform reverse flow field, but the flow quantities thus obtained should give a reasonably accurate qualitative description of the flow field.

Four-Nozzle Clusters

Nozzle shape effects, conical nozzles. - Flow-field conditions for the four-conical-nozzle cluster with the nozzles extended 1.5 inches ($S/D_E = 1.2$) are shown in figure 10. Local Mach number and total- to base-pressure ratio for the center area are presented in figure 10(a) as a function of probe position from the base plate. Actual probe locations were at $X/S = 0.42$, 0.66, 1.0, and 1.32. The total pressure $p_{t,1}$ is the measured pitot pressure corrected for normal shock losses whenever the flow Mach number was supersonic. Base pressure p_B is that measured on the base plate in the center area for the center probe and in the vent area for the vent-area probe.

In the absence of free-stream effects, nozzle-pressure ratio is the main independent variable affecting the flow field. Its effect on the base flow Mach number and total- to base-pressure ratio is shown parametrically.

For a low nozzle-pressure ratio, $p_E/p_A = 5$, the reverse flow was completely subsonic and decelerated towards the base. Increasing the nozzle-pressure ratio increased local Mach number that varied from a near sonic value downstream of the nozzle exit ($X/S > 1.0$) to a supersonic maximum that occurred near the exit plane, then decreased to subsonic values near the base. The gradual deceleration of the supersonic flow (e.g., when $p_E/p_A = 43$) is indicative of the dissipative action due to turbulent mixing and shear forces rather than a standoff shock, as previously discussed.

The point of transition from supersonic to subsonic Mach numbers occurred closer to the base as nozzle-pressure ratio increased. This is an indication of the increase in length required to decelerate the flow. Furthermore, the flow deceleration occurred more rapidly at the high pressure ratios (e.g., observe the curve for $p_E/p_A = 530$). These observations imply that at sufficiently high nozzle-pressure ratios, the supersonic flow may persist to the base plate and decelerate at the base through a normal or standoff shock.

As the probe approached the base plate, the total- to base-pressure ratio decreased from a maximum of nearly 28 times base pressure to a value equal to base pressure, and the magnitude of the total- to base-pressure ratio increased with increasing nozzle-pressure ratio. At low pressure ratios, $p_E/p_A \leq 28$, the total pressure continuously decreased, but at higher pressure ratios, the total pressure was nearly constant for $X/S \geq 1.0$ and decreased to base pressure at closer distances. The slope

of this sharply decreasing portion of the curves increases with nozzle-pressure ratio. These observations correlate with those of the flow-field Mach number to indicate that as nozzle-pressure ratio is increased, the strength of the reverse flow field increases.

Mach numbers and flow angularity in the vent area are presented in figure 10(b). Flow angles were measured relative to the base; therefore, $\alpha = 90^{\circ}$ means the flow is normal to the base. Measurements were not obtained at $X/S > 1.0$ since the probe would then be within the jet flow and improperly oriented for a description of the reverse flow. The Mach number variation was similar to that in the center area but lower in magnitude; supersonic Mach numbers were observed only for the highest nozzle-pressure ratio, $p_E/p_A = 530$. The transition to subsonic velocities occurred further from the base than in the center area (i.e., $M_L = 1.0$ at $X/S = 0.66$ in the vent area, whereas $M_L = 1.0$ at $X/S = 0.36$ in the center area). This occurrence seems reasonable since in the vent area the flow is more a function of a two-jet interaction, and the reversed flow is less confined than the four-jet interaction in the center area. At low nozzle-pressure ratios where the jet plumes are probably not impinging, $M_L = 0.1$ and $\alpha = 0^{\circ}$, which indicates very little reverse flow. As nozzle-pressure ratio increased, a stronger reverse flow occurred and turned parallel to the base at decreasing values of X/S. For example, when $p_E/p_A = 43$, the flow was nearly normal at the exit plane and was parallel to the base at $X/S = 0.42$, whereas when $p_E/p_A = 350$, the flow was probably normal to the base as close as $X/S = 0.42$.

A schematic visualization of the flow field in the center and the vent area of the four-conical-nozzle configuration is presented in figure 11. Mach number vectors (magnitude and flow angle) are presented at the jet-exit plane and at $X/S = 0.42$ for two values of p_E/p_A, a low value in figure 11(a) and a high value in figure 11(b). The flow direction in the center is always assumed near normal. For a low nozzle-pressure ratio ($p_E/p_A = 43$), the flow in the center area decelerated from a supersonic to a subsonic velocity ($M_L = 2.5$ to $M_L = 0.7$), whereas in the vent area the flow decelerated subsonically ($M_L = 0.45$ to $M_L = 0.3$) and turned from a normal direction at the exit plane to a direction parallel to the base at $X/S = 0.42$. For a high nozzle-pressure ratio ($p_E/p_A = 530$), the flow decelerated supersonically in the center ($M_L > 3.0$ to $M_L = 1.4$), whereas in the vent area the flow decelerated from a supersonic to a subsonic velocity ($M_L = 1.9$ to $M_L = 0.5$) remaining nearly normal to the base. The flow field is obviously less curved for a high nozzle-pressure ratio.

Base pressures for the four-conical-nozzle configuration with $S/D_E = 1.2$ are shown in figure 12. The ratio of base pressure to ambient pressure is plotted as a function of nozzle-pressure ratio. Symbols identify the variation in chamber pressure and location of the measurement. At a given location, the base pressure ratios for all chamber pressures tested fall on the same curve, indicating that nozzle-pressure ratio is the independent variable affecting base pressures as expected. Similarly, base pres-

sures are near or greater than ambient ($p_B/p_A \geq 1.0$), indicating jet pressurization of the base. Above $p_E/p_A = 400$, the curves become linear with a slope near 1, indicating a choked base flow condition. The center base pressures (plain symbols) are greater than those in the vent area (tailed symbols), since the flow stagnates in the center of the base.

Nozzle shape effects, contoured nozzles. - Flow-field conditions in the center area of the four-contoured-nozzle configuration, $S/D_E = 1.2$, are shown in figure 13(a). Values of p_E/p_A were greater for the contoured nozzles because of higher exit pressures at a given chamber pressure. However, the trends in both Mach number and total- to base-pressure ratio are essentially the same as with the conical nozzles (fig. 10(a)). The flow accelerated from the jet impingement point to supersonic speeds near the nozzle-exit plane and then decelerated to subsonic flow near the base, while the total pressure decreased in magnitude from the jet impingement point to the base. The magnitude of the Mach number generally appeared larger than that of the conical nozzles. For example, compare the curve for $p_E/p_A = 200$ to that of $p_E/p_A = 350$ for the conical nozzles in figure 10(a). Furthermore, at the highest pressure ratios, the precipitous decrease in both Mach number and total pressure near the base plate is indicative of a trend toward a normal shock deceleration.

Conditions in the vent area for the contoured-nozzle configuration are shown in figure 13(b). Trends and magnitudes of the local Mach number were similar to those observed in the vent area for the conical-nozzle configuration (fig. 10(b)). At low pressure ratios, the flow was subsonic; and at high pressure ratios, it accelerated to a maximum value near the exit plane and then decelerated towards the base. Local flow angularity could not be compared directly with that of the conical nozzles because of incomparable pressure ratios and limitations in the calibration. However, for a $p_E/p_A = 200$, the flow is mostly normal at $X/S > 0.42$, which agrees with observations for a nearly comparable conical nozzle $p_E/p_A = 350$. Thus, a similarity in local flow angle variations and magnitude between the two configurations is qualitatively indicated.

This similarity in flow field is further exemplified by the visualization for the contoured nozzles shown in figure 14. Comparison with that of the conical nozzles (fig. 11) shows the same variation of flow-field Mach number and flow direction from low to high values of nozzle-pressure ratio.

Base pressures for the contoured nozzles with normal base configuration are shown in figure 15. In general, base pressure ratios were less than those for conical nozzles at a given nozzle-pressure ratio. Therefore, for a given ambient pressure and nozzle-pressure ratio, base pressures for the contoured nozzles would be less than those for conical nozzles. The differences in nozzle-exit flow angles (i.e., 3.4° for the contoured nozzles compared with 12.5° for the conical nozzles) result in a lower initial flow angle for the contoured nozzles and should result in a lower base pressure as

discussed in references 2 and 6. The curves become linear at $p_E/p_A > 1000$ compared with $p_E/p_A > 400$ for the conical nozzles; thus, choking occurs at a pressure ratio higher by nearly one order of magnitude for the contoured nozzles.

Effects of nozzle gimbal. - Flow-field conditions for the contoured nozzles with 6^o outward gimbal are shown in figure 16. In general, nozzle gimbal had the effect of decreasing the magnitude of center-area Mach number and total- to base-pressure ratio, with the largest change occurring at the low pressure ratios. However, the variation of Mach number and total- to base-pressure ratio with X/S and p_E/p_A was similar in trend to the nongimbaled configuration. For example, compare the curve for p_E/p_A = 193 from figure 16(a) with the curve for p_E/p_A = 200 from figure 13(a).

The most significant change occurred in the vent area (fig. 16(b)). Not only was Mach number reduced, but at the high pressure ratios, the flow accelerated to only slightly supersonic velocities. The maximum Mach number occurred nearer the base unlike the nongimbaled configuration (fig. 13(b)) for which the maximum Mach number occurred at the exit plane. These effects are probably a result of a shift in minimum area location and the angle of jet impingement. The flow angularity indicated that the reverse flow penetrated the base region only at the highest nozzle-pressure ratio and turned parallel to the base at further distances than for the nongimbaled case. Thus, nozzle gimbal increases the flow-field curvature.

The flow visualization for the gimbaled configuration is shown in figure 17. Comparing this configuration with the nongimbaled configuration (fig. 14) clearly shows that for the gimbaled configuration at a low pressure ratio, the reverse flow is reduced in strength, the curvature is increased, and the flow in the vent area was parallel to the base even at the exit plane. At high pressure ratios, the increase in curvature is similarly evident. The center-area Mach numbers are somewhat larger for the gimbaled configuration because of the slightly larger nozzle pressure ratio (i.e., p_E/p_A = 3580 compared with p_E/p_A = 3460 for the nongimbaled configuration).

Base pressures for the gimbaled-nozzle configuration are shown in figure 18 and in general are less than values for the nongimbaled configuration (fig. 15) at a given nozzle-pressure ratio. Furthermore, choking appeared to occur at a higher nozzle-pressure ratio for the gimbaled configuration than for the nongimbaled configuration.

Effect of unextended nozzles. - The effect of locating the nozzle-exit plane flush with the base plate (i.e., $S/D_E = 0$) on flow-field conditions is shown in figure 19(a) for the conical nozzles and in figure 19(b) for the contoured nozzles. The initial point of probe travel was at the nozzle-exit plane and corresponds to X/S = 1.0 for the extended-nozzle configuration. Only data in the center area is presented. The magnitude of the Mach number varied erratically with changes in nozzle-pressure ratio for both configurations. However, in general the Mach number was subsonic at low nozzle-pressure ratios and decreased towards the base. As nozzle-pressure ratio increased, the Mach number

remained nearly constant or increased towards the base and, in general, was supersonic. Evidently the flow must decelerate at the base through a normal shock since there is not sufficient length for dissipative forces to act. The curves for the high ratios are dashed between the data for the probe position nearest the base and the stagnation point to indicate the uncertainty of the discontinuity in the curve due to the normal shock. Similarly, the curves for total- to base-pressure ratio are dashed in this region. The magnitude of the total- to base-pressure ratio increased with nozzle-pressure ratio as previously noted for the extended-base configuration, but the loss in total pressure from the impingement point to the base was not as great. In effect, these trends are similar to flow conditions downstream of the nozzle-exit plane for the extended-nozzle configuration.

Base pressures for the unextended-nozzle configurations are shown in figure 20. Conical-nozzle data are shown by the dashed line and contoured-nozzle data by the solid line. For both conical and contoured nozzles, base pressures were greater than extended-nozzle base pressure, and the choking nozzle-pressure ratio was lower than that for the extended-nozzle base.

Five-Nozzle Cluster

Flow-field Mach number in the vent area is shown in figure 21. The flow field tended to be weak with Mach numbers less than 1.0 (for $p_E/p_A < 570$ the local Mach number was near 0). The variation of Mach number and location of maximum velocity was similar to that in the vent area of the four-nozzle configuration with gimbal (fig. 16(b)). Although it is not shown, the flow direction was mostly normal to the base for all nozzle-pressure ratios tested.

Average base pressures for the five-nozzle configuration are shown in figure 22. At a given nozzle-pressure ratio, base- to ambient-pressure ratio was less than that for the four-nozzle clusters, and choking occurred at $p_E/p_A > 1000$, which is greater than that for the four-nozzle cluster. Base pressures were always near or greater than ambient pressure ($p_B/p_A > 1$) for the five-nozzle cluster as was seen for all configurations tested.

SUMMARY OF RESULTS

An experimental investigation of the base flow field for configurations of four and five clustered nozzles was made at altitudes from 60 000 to 200 000 feet utilizing conical and contoured cold flow nozzles. Measurements of flow-field Mach number, total pressure, and flow direction, as well as base pressure, indicated the following results:

Flow-Field Mach Number

1. Mach number of the reverse flow normal to the base in the center of the extended four-nozzle base increased in magnitude with increasing nozzle-pressure ratio for both conical and contoured nozzles. Values ranged from completely subsonic flow for low nozzle-pressure ratios to large regions of supersonic flow for high nozzle-pressure ratios. When supersonic flow existed, an initial sonic point occurred between the point of jet intersection and the nozzle-exit plane, and the flow accelerated to a maximum value near the exit plane. The flow then decelerated to subsonic velocities and stagnated at the base. Apparently this deceleration occurred through dissipation of the flow by shear and turbulent mixing since a base standoff shock was not observed.

2. Mach numbers in the vent area of the four-nozzle base were similar in magnitude and variation for both conical and contoured nozzles, however, the magnitudes were less than center-area values. Flow-angle measurements indicated that the flow field is curved resulting from turning of the reverse flow in exiting from the base through the vent area. This curvature decreases as nozzle-pressure ratio increases because of the increased strength of the reverse flow.

3. Outward nozzle gimbal decreased the magnitude of flow-field Mach number in both the center and the vent areas and generally resulted in more highly curved flow field.

4. The flow-field Mach number for the unextended-nozzle configuration was generally subsonic at low nozzle-pressure ratios and decreased towards the base. As nozzle-pressure ratio increased, the Mach number increased to supersonic values and either remained constant or increased towards the base. In general, these trends are similar to flow conditions downstream of the nozzle-exit plane for the extended-nozzle configuration. However, the supersonic flow decelerated at the base through a normal shock, in contrast to the extended-nozzle configuration.

5. The variation of flow-field Mach number in the vent area of the five-nozzle cluster was similar to that observed for the four-nozzle cluster with nozzle gimbal, inasmuch as the flow accelerated to low supersonic maximum velocities for high values of nozzle-pressure ratio, and this maximum occurred near the base rather than the nozzle-exit plane.

Flow-Field Total Pressure

1. Total pressure of the reverse flow normal to the base in the center of the extended four-nozzle cluster decreased in magnitude towards the base for both conical and contoured nozzles. Total pressure decreased from values as high as 28 times the

base pressure to a value equal to base pressure, and the magnitude of the loss tended to increase with increasing nozzle-pressure ratio. This loss is contrary to previous assumptions of a constant total pressure in the reverse flow and is related to shear and mixing losses in the reverse flow.

2. Similar trends were seen for the gimbaled nozzle and unextended-base configurations. The magnitude of the total pressure loss, however, was generally less than that for the nongimbaled extended-nozzle configuration. For the unextended-base configuration, an additional loss occurred, because of normal shock deceleration of the supersonic flow.

Base Pressures

1. Base pressures for all configurations tested were near or greater than ambient pressure at all values of nozzle-pressure ratio, indicating that the base was pressurized by the recirculating flow.

2. The use of contoured nozzles resulted in lower base pressures than those for conical nozzles at a given altitude and nozzle-pressure ratio. In addition, the nozzle-pressure ratio at which the base flow choked was nearly one order of magnitude higher for the contoured nozzles.

3. Nozzle gimbal decreased the base pressure and increased the choking nozzle-pressure ratio. However, an unextended base resulted in base pressures that were greater than those for the normal base, and choking occurred at a lower nozzle-pressure ratio.

4. The five-nozzle configuration had lower base pressures, at a given altitude and nozzle-pressure ratio, than the four-nozzle configurations, and choking occurred at a higher nozzle-pressure ratio.

Lewis Research Center,
National Aeronautics and Space Administration,
Cleveland, Ohio, December 12, 1966,
124-10-02-01-22.

REFERENCES

1. Korst, H. H.; and Chow, W. L.: Compressible Non-Isoenergetic Two-Dimensional Turbulent (Prt = 1) Jet Mixing at Constant Pressure - Auxiliary Integrals, Heat Transfer and Friction Coefficients for Fully Developed Mixing Profiles. Rep. No. TN 392-4, University of Illinois, Eng. Exp. Station, Dept. Mech. Eng., Jan. 1959. (Available from DDC as AD-211328.)

2. Goethert, B. H.: Flow Characteristics and Performance of Multi-Nozzle Rocket Exhausts. Simulated Altitude Testing of Rockets and Missile Components, Symposium Proceedings. Rep. No. TR 60-6, Arnold Engineering and Development Center, Mar. 1960, pp. 3-4-1 to 3-4-36.

3. Goethert, B. H.; and Barnes, L. T.: Some Studies of the Flow Pattern at the Base of Missiles with Rocket Exhaust Jets. Rep. No. TR 58-12 rev., Arnold Engineering and Development Center, June 1960.

4. Marion, E. D.; Danield, D. J.; Herstine, G. L.; and Burge, G. W.: Exhaust Reversal from Cluster Nozzles - A New Flow Model. Paper No. 2706-62, ARS, Nov. 13-18, 1962.

5. Dailey, C. L.; and Wood, F. C.: Computation Curves for Compressible Fluid Problems. John Wiley & Sons, Inc., 1949.

6. Baughman, Eugene L.; and Kochendorfer, Fred D.: Jet Effects on Base Pressures of Conical Afterbodies. NACA RM E57E06, 1957.

7. Warren, Walter R., Jr.: The Mixing of an Axially Symmetric Compressible Jet with Quiescent Air. Rep. No. AER No. 252, Princeton University, Sept. 30, 1953.

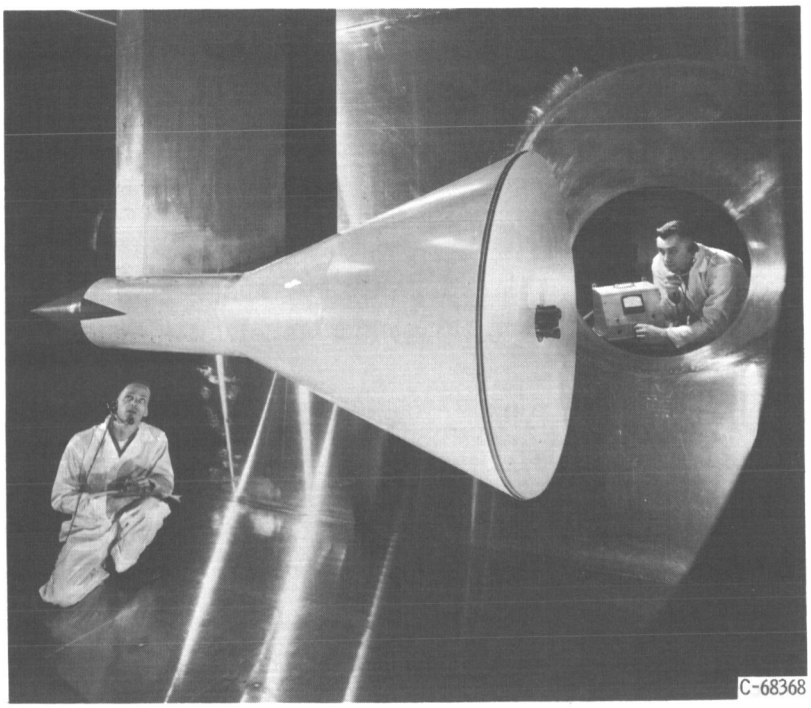

Figure 1. - Model installed in Lewis 10- by 10-foot supersonic wind tunnel.

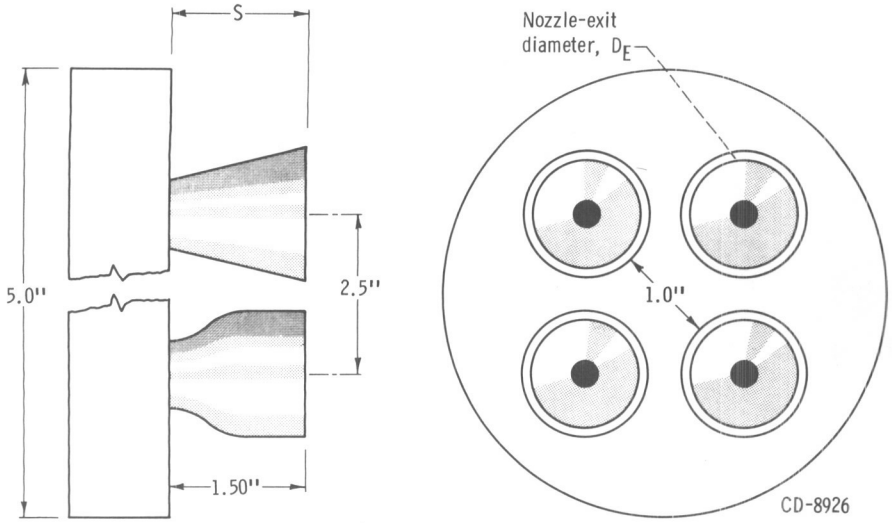

(a) Normal base showing both contoured and conical nozzles.

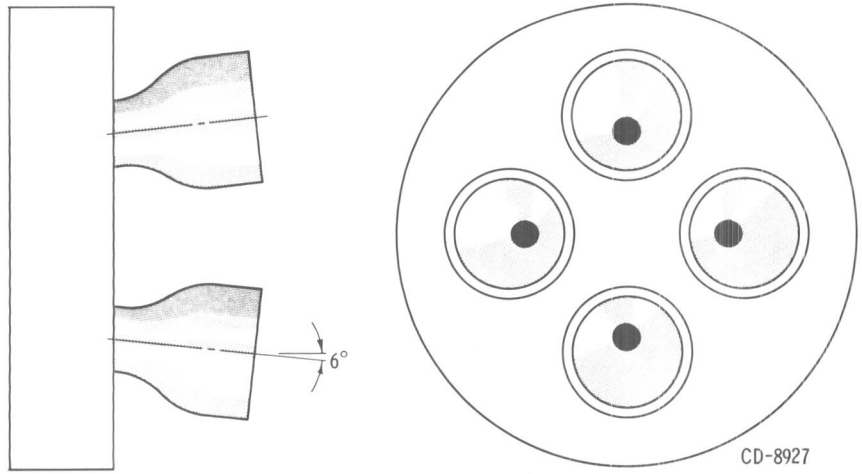

(b) Gimbaled base, 6° outward-gimbaled contoured nozzles.

(c) Unextended nozzles.

Figure 2. - Four-nozzle base configurations. Nozzle-extension ratio S/D_E, 1.2.

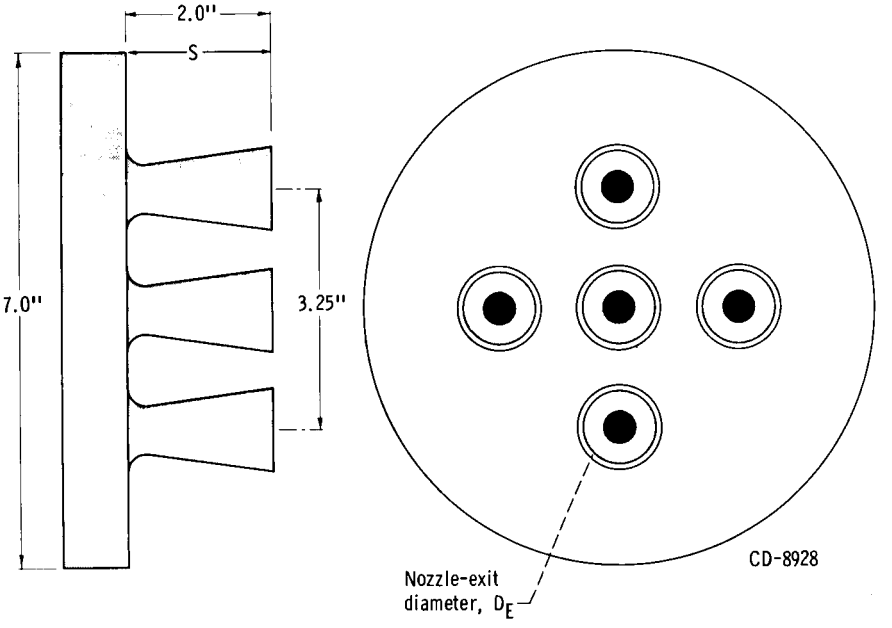

Figure 3. - Five-nozzle base configuration. Nozzle-extension ratio S/D_E, 2.0.

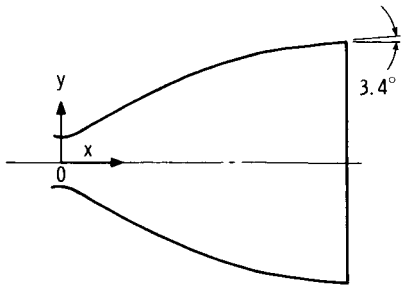

Station	
x, in.	y, in.
0	0.125
.0675	.1438
.125	.1775
.250	.2475
.375	.3135
.500	.375
.625	.430
.750	.480
.875	.521
1.000	.558
1.125	.5835
1.250	.605
1.375	.618
1.500	.625

(a) Interior contour of bell-shaped nozzle used in four-nozzle cluster. Nozzle-area ratio, 25.

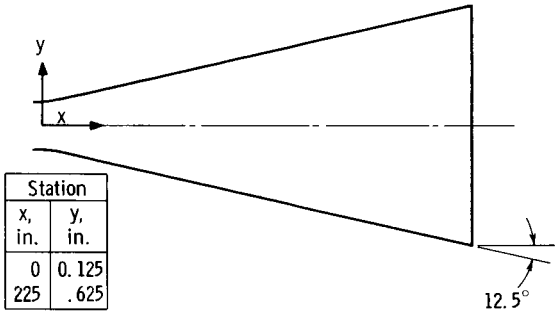

Station	
x, in.	y, in.
0	0.125
225	.625

(b) Conical nozzle used in four-nozzle cluster. Nozzle-area ratio, 25; contour, 12.5° half-angle cone.

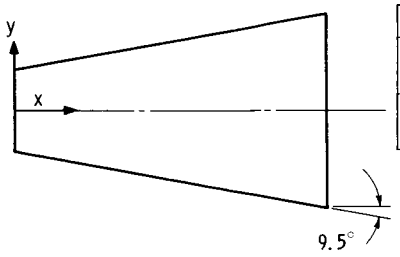

Station	
x, in.	y, in.
0	0.2255
1.64	.50

(c) Conical nozzles used in five-nozzle-cluster test. Nozzle-area ratio, 4.92.

Figure 4. - Nozzle details.

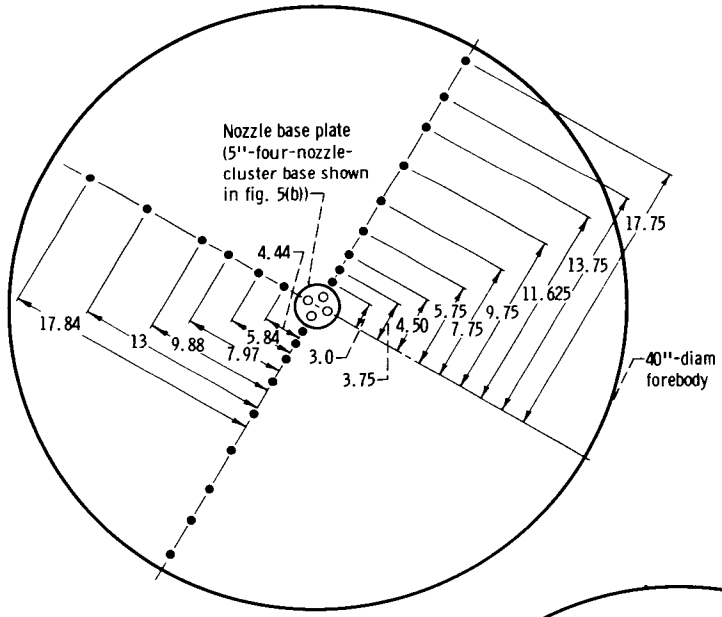

(a) Forebody base.

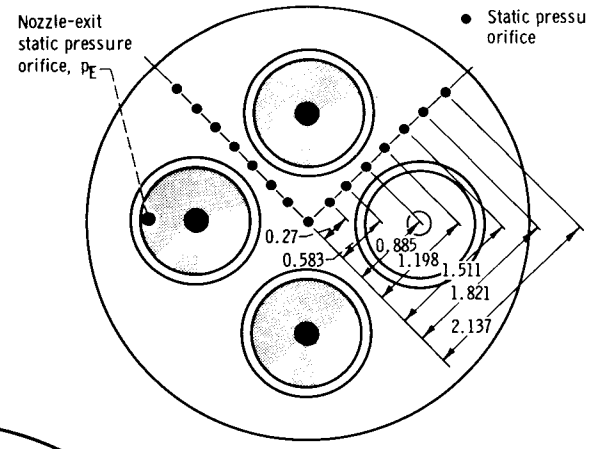

(b) Four-nozzle base plate.

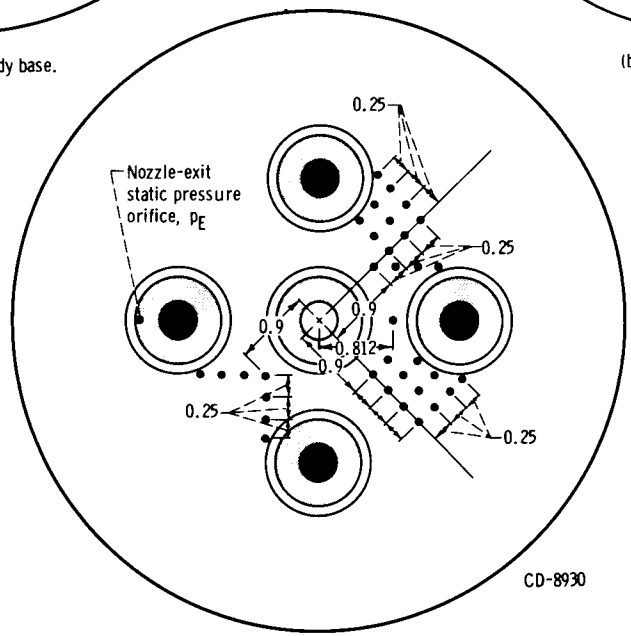

(c) Five-nozzle base plate.

Figure 5. - Pressure instrumentation locations. All dimensions in inches.

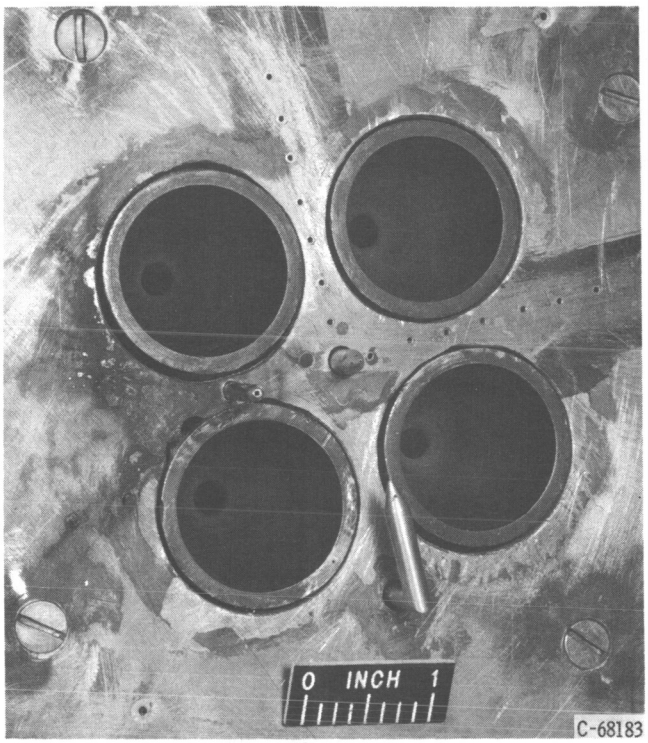

(a) Four-nozzle cluster.

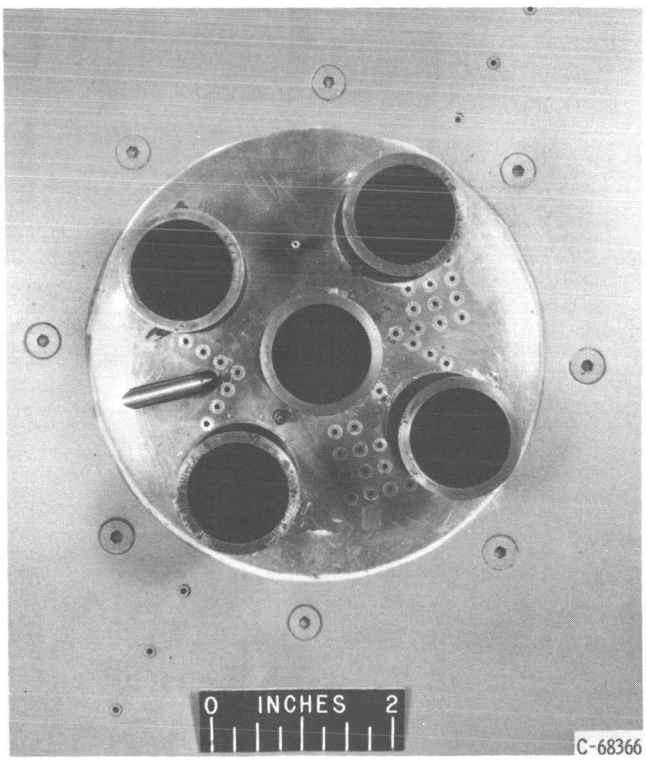

(b) Five-nozzle cluster.

Figure 6. - Probe locations.

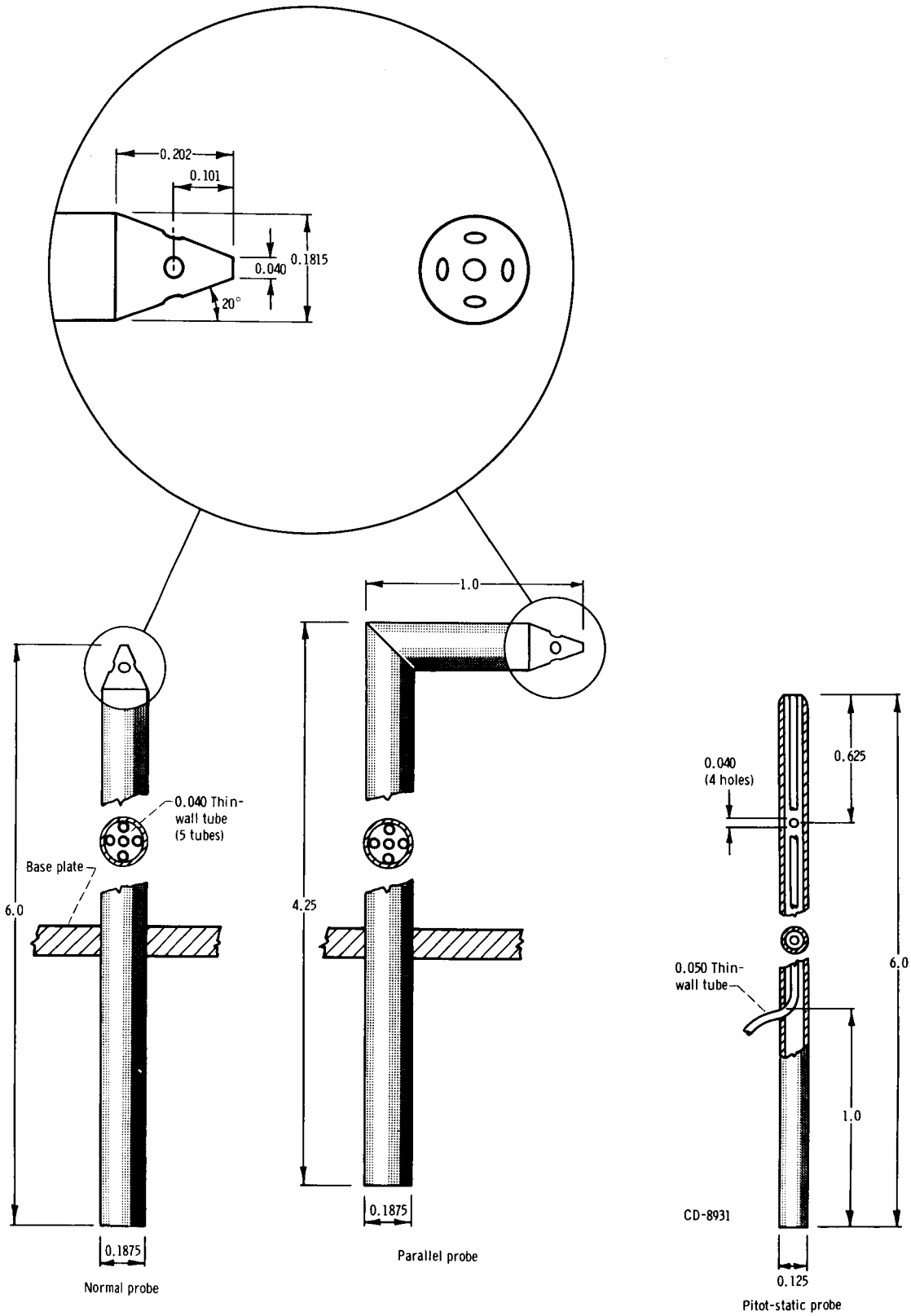

Figure 7. - Probe design details. All linear dimensions are in inches.

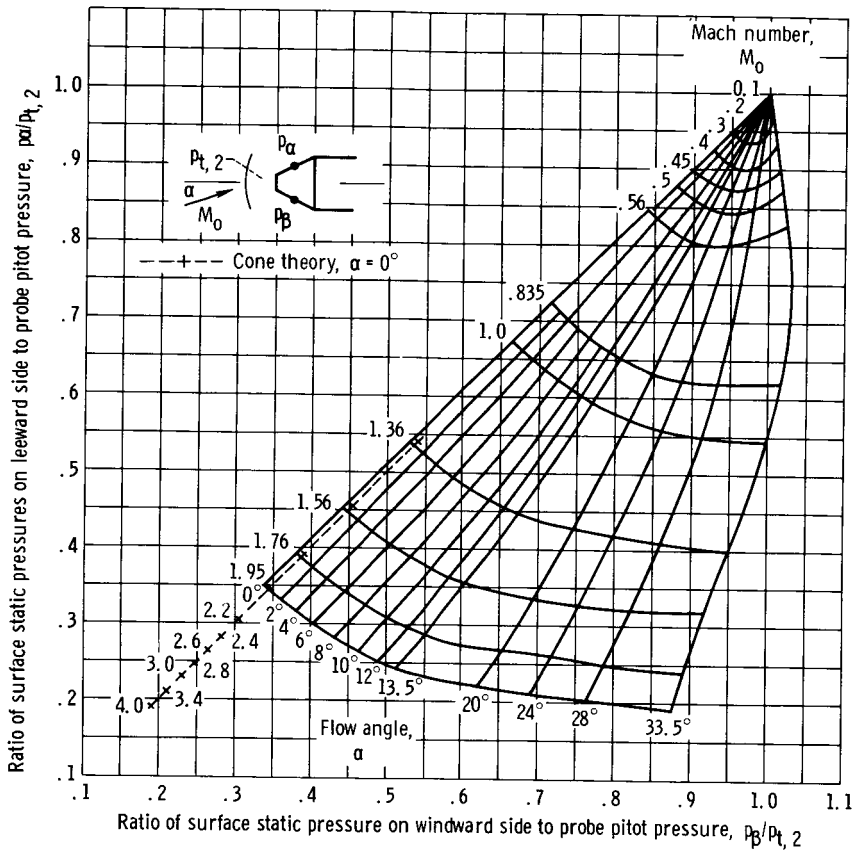

Figure 8. - Conical probe calibration.

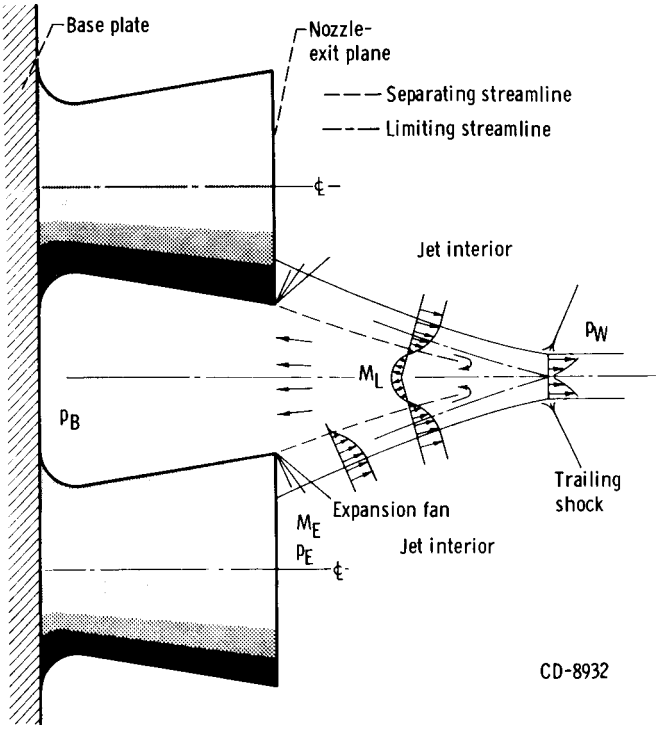

Figure 9. - Theoretical flow model (ref. 6).

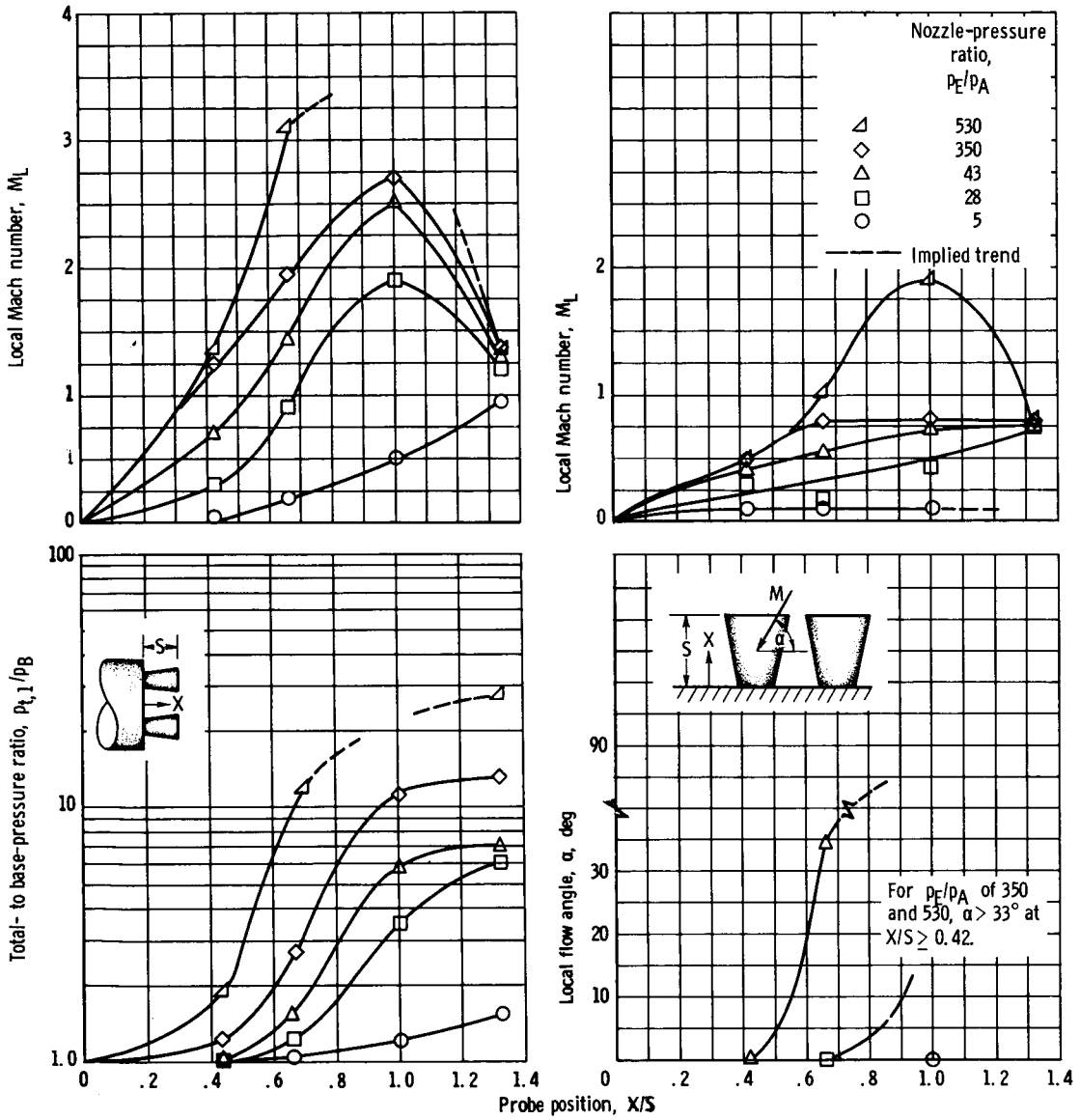

(a) Center area. Nozzle extension beyond base, 1.5 inches.

(b) Vent area.

Figure 10. - Flow field conditions for four-conical-nozzle configuration. Nozzle-extension ratio, 1.2; nozzle-area ratio, 25.

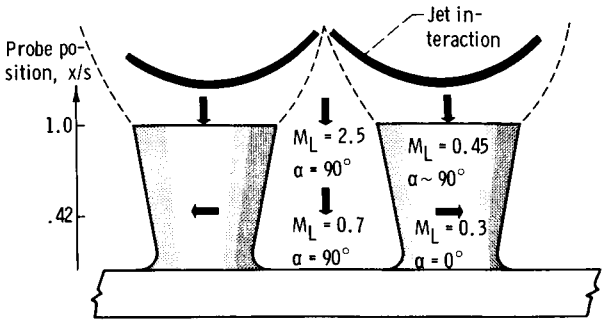

(a) Nozzle-pressure ratio p_E/p_A, 43.

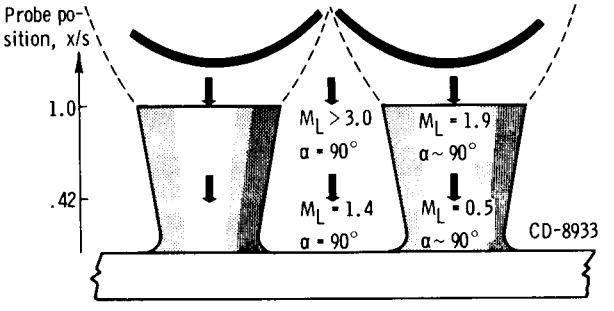

(b) Nozzle-pressure ratio p_E/p_A, 530.

Figure 11. - Flow-field visulation for four-conical-nozzle configuration. Nozzle-extension ratio, 1.2; nozzle-area ratio, 25.

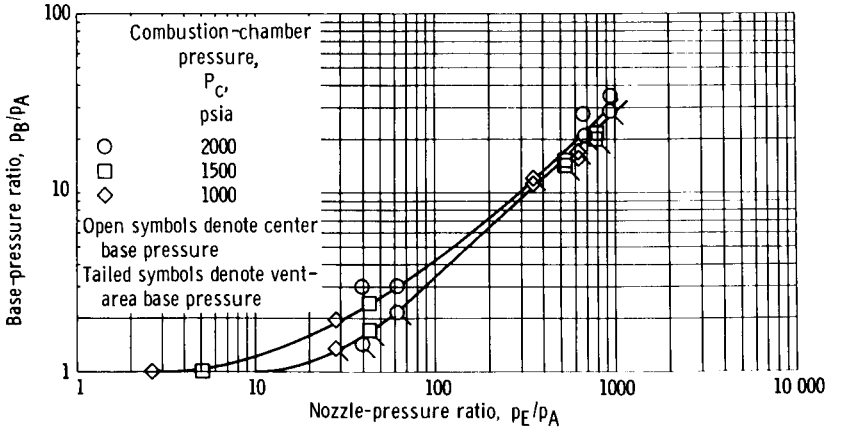

Figure 12. - Base pressures for four-conical-nozzle configuration. Nozzle-extension ratio, 1.2; nozzle-area ratio, 25.

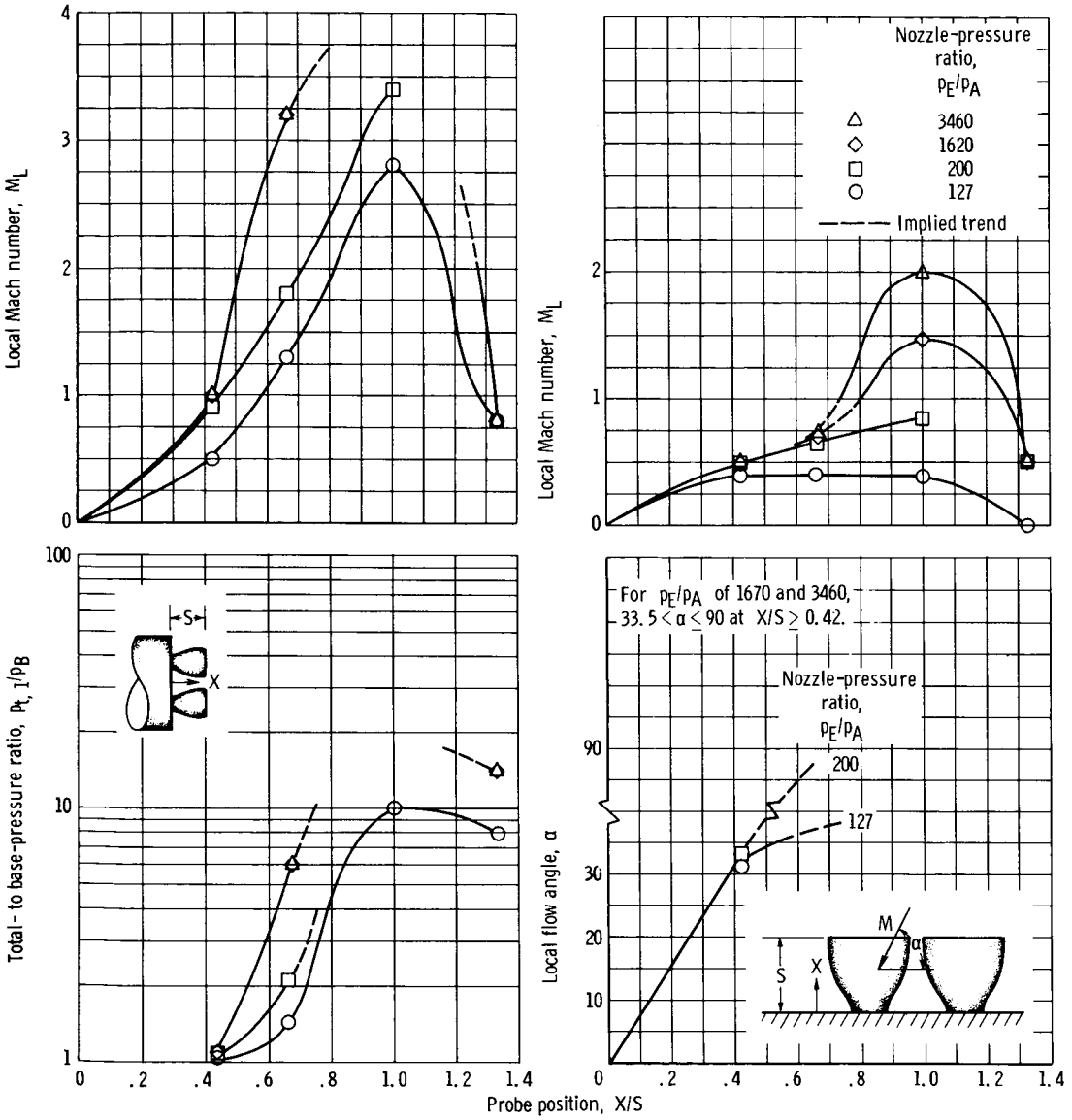

(a) Center area.

(b) Vent area.

Figure 13. - Flow-field conditions for four-contoured-nozzle configuration. Nozzle-extension ratio, 1.2; nozzle-area ratio, 25.

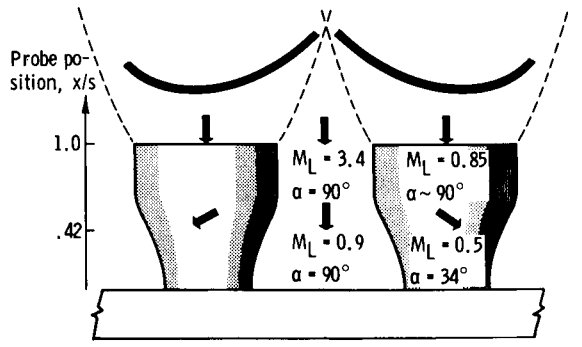

(a) Nozzle-pressure ratio p_E/p_A, 200.

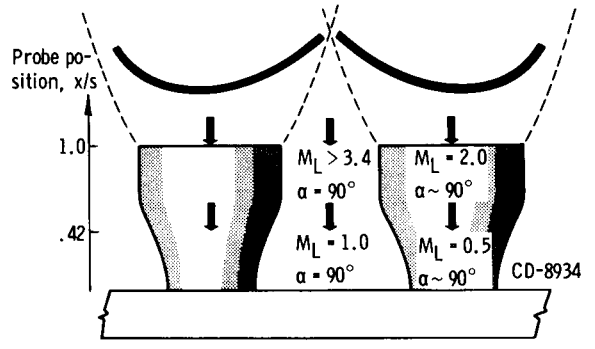

(b) Nozzle-pressure ratio p_E/p_A, 3460.

Figure 14. - Flow field visualization for four-contoured-nozzle configuration. Nozzle-extension ratio, 1.2; nozzle-area ratio, 25.

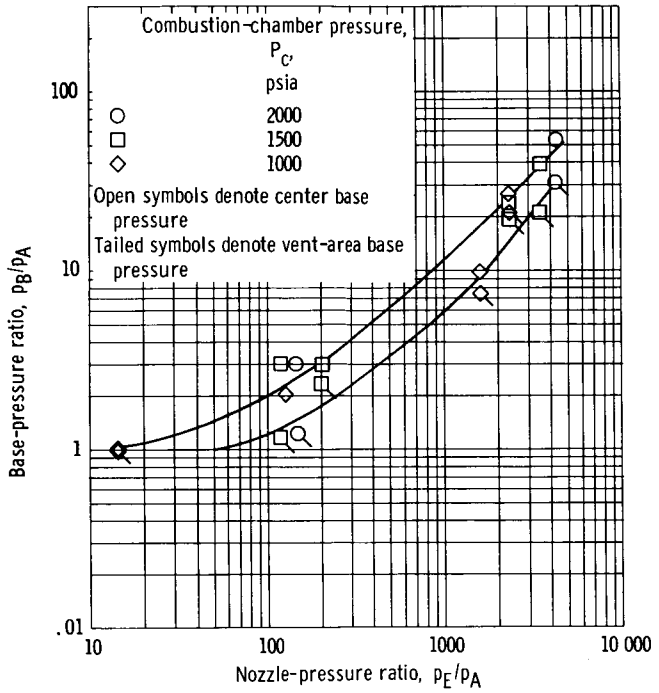

Figure 15. - Base pressures for four-contoured-nozzle configuration. Nozzle extension ratio, 1.2; nozzle-area ratio, 25.

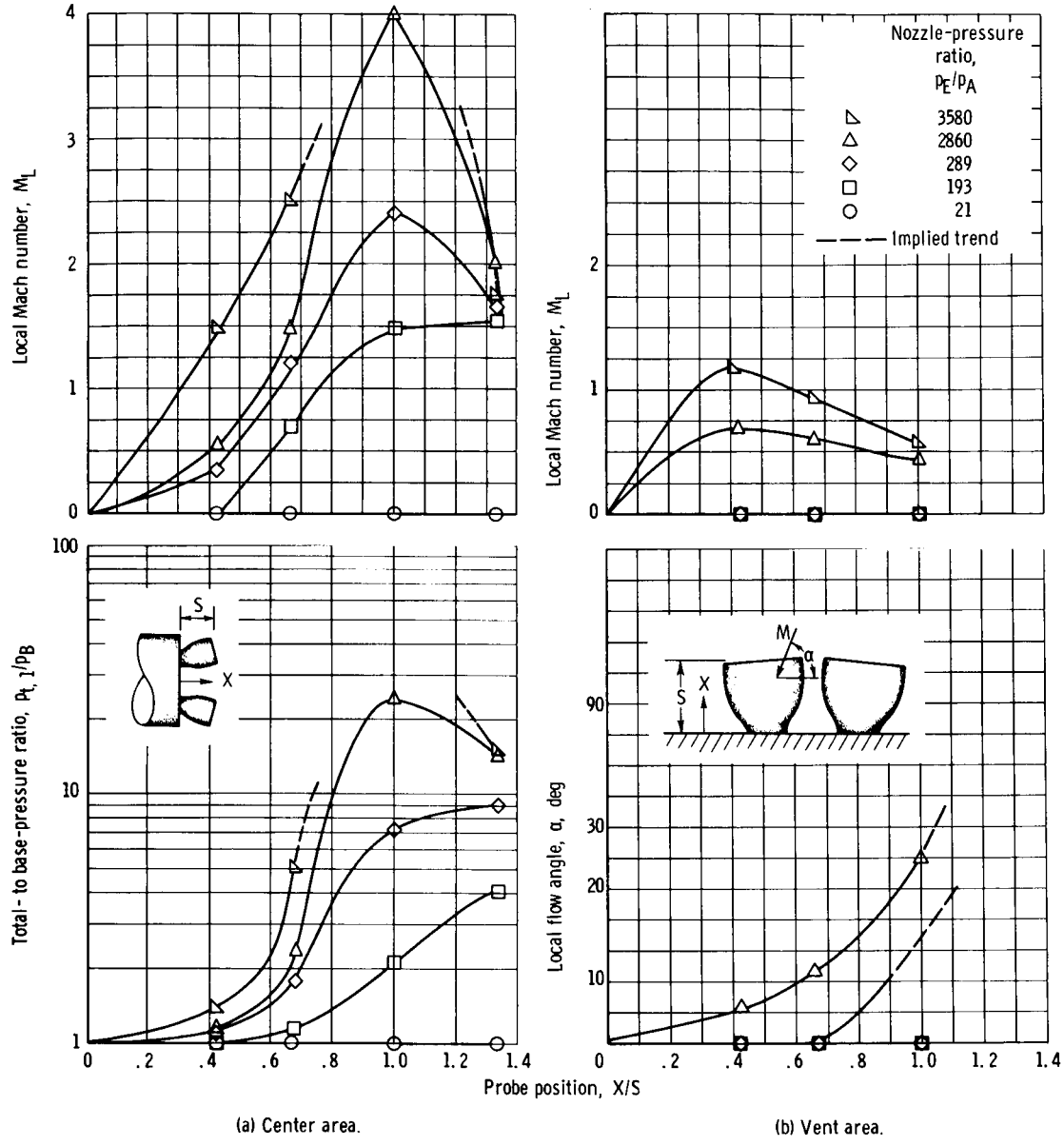

Figure 16. - Flow-field conditions for four-contoured-nozzle configuration, gimbaled nozzles. Nozzle-extension ratio, 1.2; nozzle-area ratio, 25.

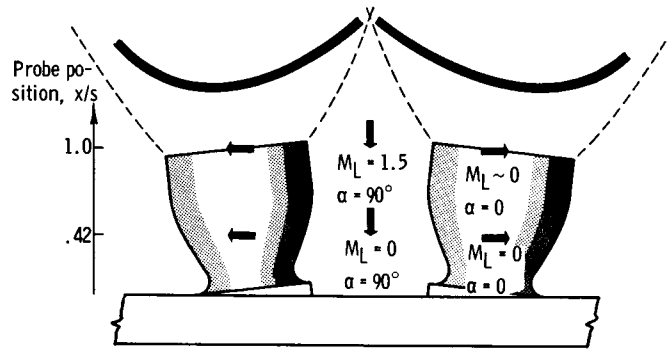

(a) Nozzle-pressure ratio p_E/p_A, 193.

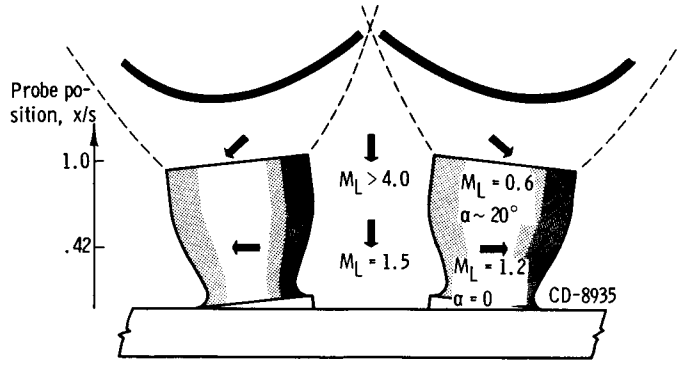

(b) Nozzle-pressure ratio p_E/p_A, 3580.

Figure 17. - Flow field visualization for four-contoured-nozzle configuration, gimbaled nozzles. Nozzle-extension ratio, 1.2; nozzle-area ratio, 25.

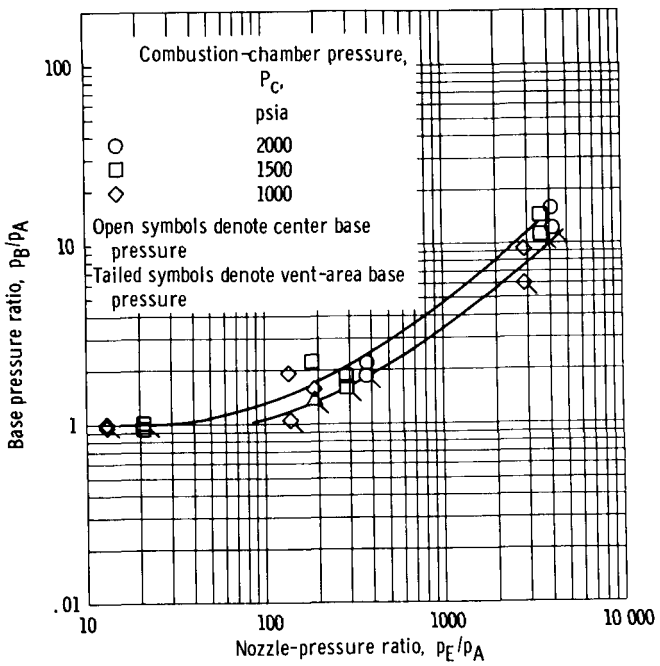

Figure 18. - Base pressures for four-contoured-nozzle configuration, gimbaled nozzles. Nozzle-extension ratio, 1.2; nozzle-area ratio, 25.

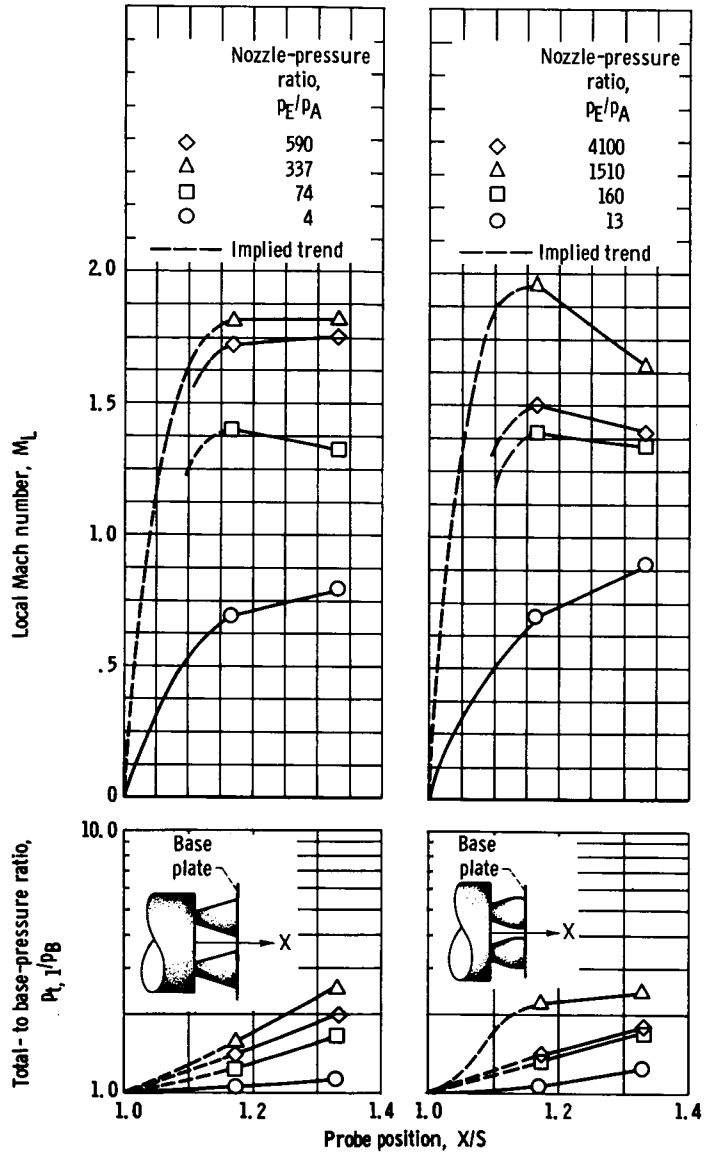

(a) Four conical nozzles. (b) Four contoured nozzles.

Figure 19. - Flow-field Mach number and total pressure in center area for unextended-nozzle configuration. Nozzle-extension ratio, 0; nozzle-area ratio, 25.

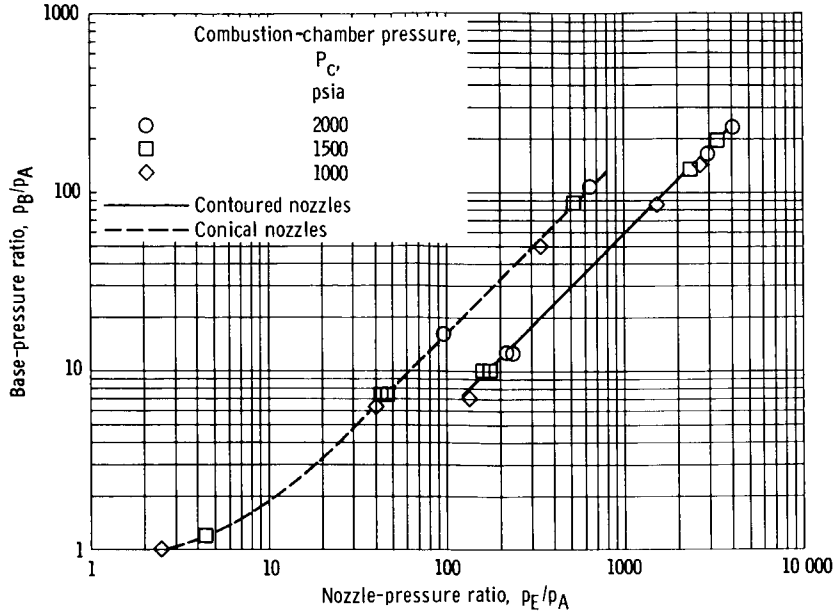

Figure 20. - Center base pressures for unextended nozzle configurations. Nozzle-extension ratio, 0; and nozzle-area ratio, 25 for both conical and contoured nozzles.

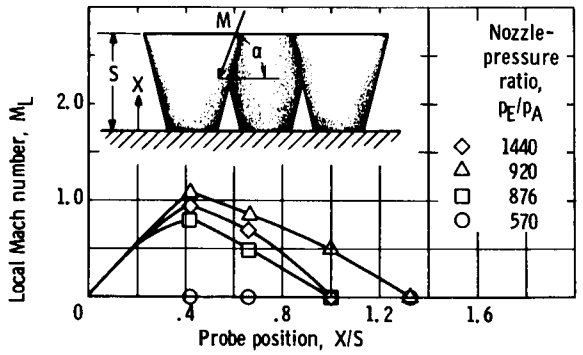

Figure 21. - Mach number in vent area for five-nozzle configuration. Nozzle-extension ratio, 2.0; and nozzle-area ratio, 4.92. Local Mach number is 0 at all probe positions for nozzle-pressure ratio $\leq$ 570.

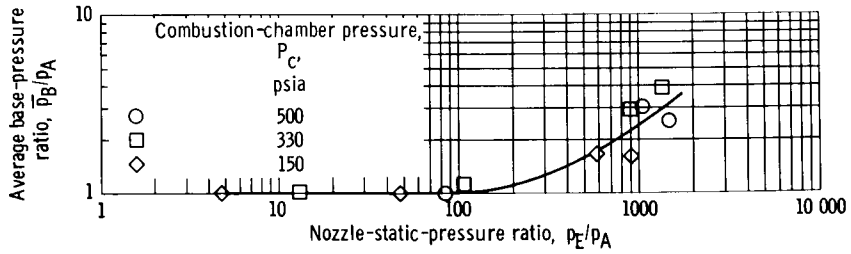

Figure 22. - Average base pressures for five-nozzle configuration. Nozzle-extension ratio, 2.0; nozzle-area ratio, 4.92.

NASA-Langley, 1967 —— 1